Stabilization of highly efficient and stable phase-pure $FAPbI_3$ Perovskite Solar Cells by Molecularly Tailored 2D-Overlayers

Yuhang Liu[1†], Seckin Akin[1,4†], Alexander Hinderhofer[2], Felix T. Eickemeyer[1], Hongwei Zhu[1], Ji-Youn Seo[1], Jiahuan Zhang[3], Frank Schreiber[2], Hong Zhang[1], Shaik M. Zakeeruddin[1], Anders Hagfeldt[3], M. Ibrahim Dar[1*], Michael Grätzel[1*]

[1]*Laboratory of Photonics and Interfaces, Department of Chemistry and Chemical Engineering, École Polytechnique Fédérale de Lausanne, Lausanne CH-1015, Switzerland.*
[2]*Institut für Angewandte Physik, Universität Tübingen, 72076 Tübingen, Germany.*
[3]*Laboratory of Photomolecular Science, École Polytechnique Fédérale de Lausanne, Station 6, CH-1015 Lausanne, Switzerland.*
[4]*Department of Metallurgical and Materials Engineering, Karamanoglu Mehmetbey University, Karaman, Turkey.*

Correspondence to: ibrahim.dar@epfl.ch (M.I.D.); michael.graetzel@epfl.ch (M.G.)

[†]These authors contributed equally to the work.

Abstract

Due to their attractive optolectronic properties, metal halide APbI3 perovskites employing formamidinum (FA^+) as A cation are presently the focus of intense research, The superior chemical and thermal stability of FA^+ cations renders α-$FAPbI_3$ more suitable for solar cell applications than methylammonium lead iodide ($MAPbI_3$). However, its spontaneous conversion to the yellow non-perovskite phase (δ-$FAPbI_3$) under ambient conditions poses a serious challenge for practical applications. Here, we report on the stabilization of the desired α-$FAPbI_3$ perovskite phase by protecting it with a two-dimensional (2D) $IBA_2FAPb_2I_7$ (IBA = *iso*-butylammonium overlayer, formed *via* stepwise annealing. Remarkably, the α-$FAPbI_3$/$IBA_2FAPb_2I_7$ based perovskite solar cell (PSC) reached a high power conversion efficiency (PCE) of close to 23 %. In addition, it showed excellent operational stability, retaining ~85% of its initial efficiency under severe combined heat and light stress, i.e. simultaneous exposure with maximum power tracking to full simulated sunlight at 80 °C over a period of 500 h.

Introduction

Due to their high power conversion efficiency (PCE) exceeding already 25 % and ease of production, hybrid organic metal halide perovskite solar cells (PSCs) are presently attracting wide attention both from the scientific community and photovoltaic industry (*1-7*). Most PSCs employ formulations containing methylammonium (MA^+) cations which however are unstable decomposing to methylamine upon exposure to heat, moisture, and light (*8-13*). Therefore, for the large-scale deployment of highly-efficient PSCs, the intrinsic instability issues associated with the loss of MA^+ cations need to be mitigated (*7, 14-20*). In this regard, formamidinium (FA^+) cations offers an attractive alternative to MA^+ as pristine $FAPbI_3$ features a lower volatility and close to optimal Goldschmidt tolerance factor (*21*). as well as an absorption edge extending into the near IR to ~840 nm. rendering pristine $FAPbI_3$ a more efficient solar light than MAPbI3 (*4, 22, 23*). However, the

spontaneous formation of the photovoltaically inactive, non-perovskite yellow phase (δ-$FAPbI_3$) below the α to δ phase transition at 170 ºC (*16, 24*) causes a serious predicament. introducing Cs^+, or MA^+ into the $FAPbI_3$ lattice prevents the formation of its delta phase, However, the incorporation of these ions affects the spectral response and operational stability of the resulting PSCs under heat stress and in humid conditions (*4, 25-27*).

Here we achieve stabilizeation of the α-$FAPbI_3$ phase by introducing a stepwise annealing process and covering it with a novel two-dimensional $IBA_2FAPb_2I_7$ (n = 2) perovskite layer containing iso-butylammonium (IBA) as a spacer layer. The confluence of stepwise annealing and $IBA_2FAPb_2I_7$ lamination allowed the formation of pristine α-$FAPbI_3$ films containing long-lasting charge-carriers with lifetime exceeding 1.5 µs. These desired structural and spectral features translated into high photovoltage of 1113 mV as compared to 1053 mV for reference, leading to the realization of a PCE close to 23%, a record for $FAPbI_3$ –based PSCs. Remarkably we achieved excellent operational stability, the PSCs retaining ~95% of their initial efficiency at the maximum power point (MPP) under full-sun illumination over 700 h. The superior robustness of the $FAPbI_3$ protected by the 2D overlayer was further confirmed by long term testing under harsh simultaneous heat and light stress. These devices showed only small degradation under full-sun illumination for 500 hours at 80°C, while unprotected $FAPbI_3$ films lost rapidly over 60% of their initial performance.

Results and discussion

Stepwise annealing for high-quality $FAPbI_3$ perovskite film

We employed methylammonium chloride (MACl) (*28*) as a crystallization aid to form films of pure a-$FAPbI_3$ containing only trace amounts of yellow δ-$FAPbI_3$ phase as established by grazing incidence wide angle synchrotron X-Ray diffraction (GIWAX), and absorption and photoluminescence analysis (*28*). Details are presented in **Supplementary Note 1** and **Figure S2 – S5**. Top-view scanning electron microscopy (SEM) pictures of the $FAPbI_3$ perovskite films with and without MACl treatment are shown in **Figure 1a** and **Figure S1**, respectively and reveal that the MACl treatment reduces their surface roughness. To probe the formation of δ-$FAPbI_3$ phase, x-ray diffraction (XRD) patterns were recorded, and the results are shown in **Figure 1b**. The $FAPbI_3$ films formed in the absence of MACl exhibit a peak at $2\theta = 11.6^o$, resulting from the presence of δ-phase. By contrast, MACl-treated $FAPbI_3$ did not show these δ-$FAPbI_3$ reflections. However, the formation of large pinholes is apparent presumably related to the rapid release of gaseous MACl. Such pinholes mostly cause shunts resulting in low PCEs and poor stability (**Figure S6**). To prevent their formation we applied a stepwise annealing procedure as shown in **Figure S7**. An intermediate annealing step at 120 ºC for a duration of 5 min substantially reduced the amount of pin holes in the $FAPbI_3$ perovskite film as shown in **Figure 1c**. Finally, we obtained smooth and conformal $FAPbI_3$ perovskite films composed of micron-sized grains as shown in **Figure 1d** by optimizing a three-step annealing procedure.

Power conversion efficiencies (PCE) obtained with such films using the FTO/TiO_2/perovskite/spiro-OMeTAD/Au architecture are shown in **Table 2** We achieved a maximum PCE of ~ 20.4% with such MACl-treated and stepwise annealed $FAPbI_3$ perovskite films. In contrast, PSCs made without the stepwise annealing procedure yielded a PCE of only 16.5% due to a significantly lower open circuit voltage (V_{OC}) and fill factor (FF) ascribed to the poor film quality.

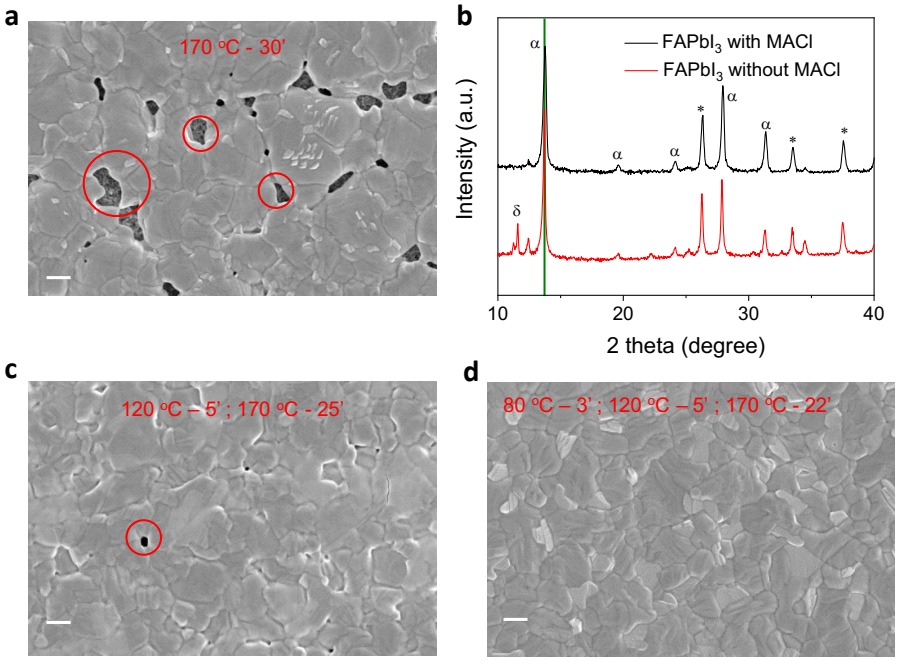

Figure 1a, Morphological and structural analysis: Single-step annealing treatment, **b**, XRD patterns of $FAPbI_3$ perovskite with and without MACl treatment. **c**, two-step annealing treatment and **d**, three-step annealing treatment. Representative pinholes are highlighted in red circle, and the scale bars represent 500 nm in length.

Surface treatment and structural characterization of $FAPbI_3$ –based perovskite

Although the as-prepared $FAPbI_3$ perovskite films were phase pure (See **supplementary note 1**) and yielded PCEs of up to 20.4%, prolonged exposure to ambient air led to the formation of photo-inactive phases, i.e. PbI_2 and δ-$FAPbI_3$ as shown in **Figure S8**. To avoid this degradation and further improve the PCE, we introduced iso-butylammonium iodide (IBAI) as to form a 2D-protective layer on top of the 3D α– $FAPbI_3$phase (**Figure 2a**). Our treatment involved spin-coating a 30 mM solution of IBAI in isopropanol on the surface of as-prepared $FAPbI_3$ perovskite films followed by annealing at 110 °C for 10 min. We ascertained by SEM that this treatment did not alter the morphology of the underneath photoactive layer (**Figure S9**).

We investigated the structure of the overlayer formed by the IBA surface treatment using grazing incidence wide-angle X-ray scattering (GIWAXS) and present data in **Figure 2b.** The GIWAXS reflections show distinct diffraction patterns, which we indexed to the structure of the 2D-perovskite IBA_2PbI_4. **Table 1**. summarizes the orthorhombic unit cell dimensions derived from fitting the GIWAXS data. For comparison, we show also the unit cell parameters of the previously reported structural analogous butylammonium lead iodide (BA_2PbI_4) (*29*). Compared to the BA_2PbI_4, the unit cell of IBA_2PbI_4 is smaller, mainly because the long unit cell axis is shortened by 1.5 Å, which is consistent with the alkyl chain length difference in the two organic spacer molecules.

Table 1, unit cell parameters of BA_2PbI_4 (*29*) and IBA_2PbI_4 based 2D perovskites.

2D Perovskite	***a***	***b***	***c***	**Volume**
2D-BA_2PbI_4 (*29*)	8.87	8.69	27.6	2129
2D-IBA_2PbI_4	8.9	8.7	26.2	2029

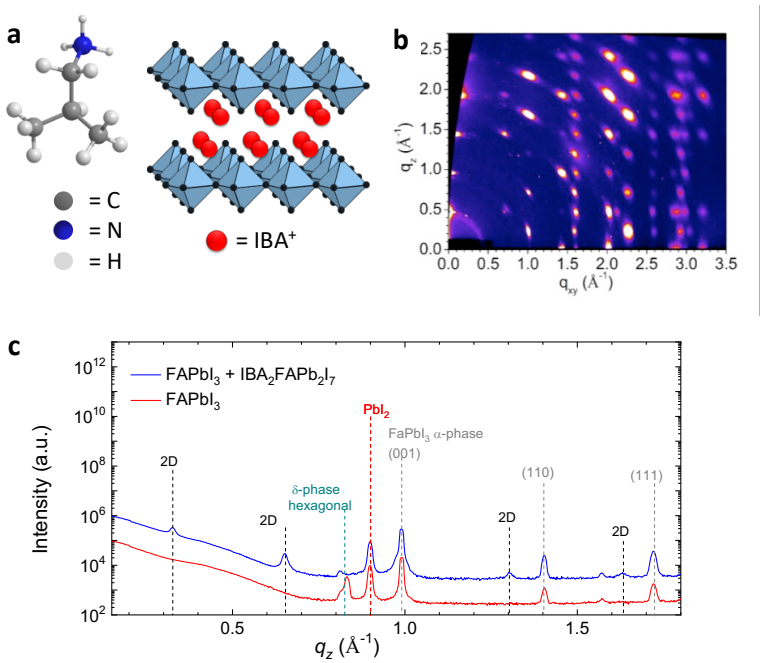

Figure 2. a, Chemical structure of IBA^+ and schematic illustration of pure 2D perovskite based on IBAI. **b**, GIWAXS data of pure 2D-IBA_2PbI_4 (angle of incidence = 0.14°). **c**, XRD data of a bare $FAPbI_3$ film, and $FAPbI_3$/2D-$IBA_2FAPb_2I_7$ prepared by the stepwise annealing method.

XRD data of pristine and IBAI treated $FAPbI_3$ films are shown in **Figure 2c**. Each film exhibits structural features corresponding to the α-$FAPbI_3$ perovskite phase with a lattice spacing of 6.36 Å (*30*), the hexagonal $FAPbI_3$ (non-perovskite phase) (*31*) and PbI_2. The IBAI treated $FAPbI_3$ films revealed the formation of $IBA_2FAPb_2I_7$ overlayer exhibiting reflections of the 2D-structure with a lattice spacing of 38.56 Å (**Table 1**). We assume some FA of the underlying 3D structure to be used up in the formation of the $IBA_2FAPb_2I_7$ (n = 2) layer. The lattice spacing is slightly smaller than the lattice spacing of the $BA_2FAPb_2I_7$ (n = 2) structure of 39.35 Å (*32*), which is consistent with the length difference in the spacer molecules BAI and IBAI. To the best of our knowledge, this is the first investigation of iso-butanol as spacer layer in 2D metal halide perovskites. Cho et.al (*33*) used mixtures of n-butyl and iso-butylammonium cations for surface passivation treatments yielding a PCE of 21.7% mixed cation.

GIWAXS data of pristine and IBAI treated $FAPbI_3$ films (**Figure 3a** and **3b)** confirm the formation of α-$FAPbI_3$ perovskite-phase in agreement with the XRD measurements. The additional 2D reflections (**Figure 3b**) arising from the 2D-$IBA_2FAPb_2I_7$ overlayer are along the q_z axis indicating their orientation to be parallel to the substrate. With the radially integrated data over the measured q-space, (**Figure 3c**) we can qualitatively estimate the amount of PbI_2 and hexagonal phase $FAPbI_3$ in the scattering volume. In the sample with 2D-$IBA_2FAPb_2I_7$ overlayer a negligible content of the hexagonal polymorph and a smaller amount of excess PbI_2 compared to the non-covered sample is observed.

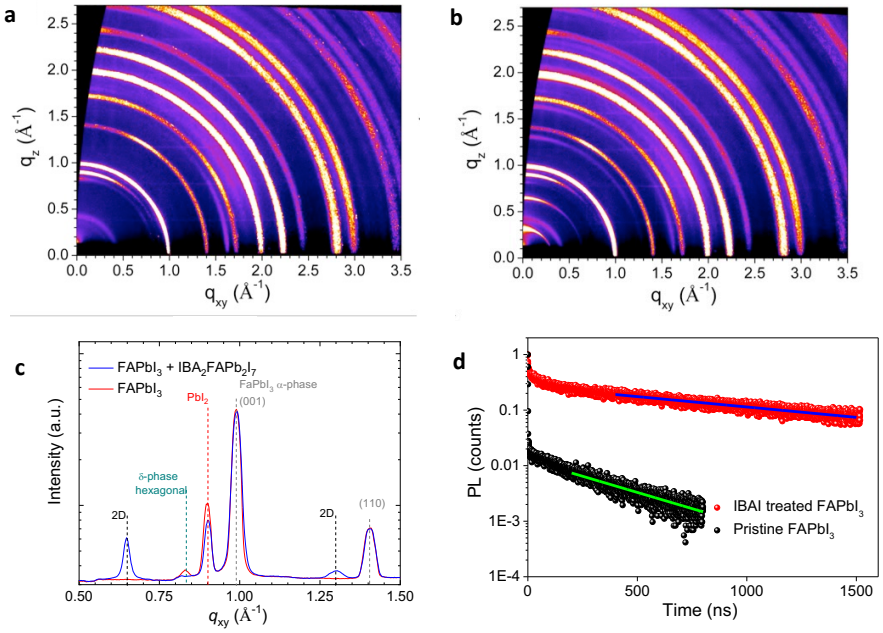

Figure 3: Structural and spectroscopic characterization. GIWAXS data of (**a**) $FAPbI_3$ film (**b**) $FAPbI_3$/2D $IBA_2FAPb_2I_7$. Angle of incidence was 0.14°. **c** Radially integrated GIWAXS data from Figures a)-b) and d), TRPL results of neat $FAPbI_3$, and $FAPbI_3$/$IBA_2FAPb_2I_7$ – based perovskites. The blue and green curves are fits to the kinetic model published previously. (*34*). Both cases (k = 0 and S = 0 for FBAI treated films) result in the same fit.

Charge-carrier dynamics

We further investigated the impact of the $IBA_2FAPb_2I_7$ layer on the optoelectronic properties of the α-$FAPbI_3$ perovskite films using time-resolved photoluminescence (TRPL) as shown in Fig. 3d. Both the untreated and treated films show two distinct decay regimes. A very fast decay within the first 10 ns is followed by a slow monexponential decay. The fast decay at early times is caused by carrier diffusion due to the initial exponential excitation profile in combination with charge carrier trapping very likely caused by shallow traps on or near the surface (PbI_2, δ-$FAPbI_3$ non-perovskite phase or surface states). The IBAI treated film shows a slower decay by more than one order of magnitude within the first 10 ns compared to the untreated film. Since the carrier diffusion rate is the same in both films, we infer that the IBAI treatment alters the defect chemistry of the surface which leads to a significantly lower trap density. Also the first order decay kinetics at times > 10 ns are much slower for the treated than the untreated films. We applied numerical simulations to analyze the different decay kinetis . Details for this simulation can be found in Zhu et al (*34*). The single exponential decay can be caused by either pseudo first SRH recombination with a recombination constant k_1 or by surface recombinations with a surface recombination velocity S. Since both films have the same bulk material and, hence, the same k_1, the only difference lies in S. We considered two extreme cases for the IBAI treated film, where in the first case the film exhibits no bulk recombinations ($k_1 = 0$), i.e. the monoexponential decay is exclusively caused by surface recombination. Conversely, in the second case we assume that the film exhibits no surface recombination (S = 0), i.e. the decay is solely caused by SRH type bulk recombination.. From this

we calculated the difference in velocity of surface recombination for the two films to be ΔS = 32 cm/s which is the same in both extreme cases. The details of this calculation can be found in **Table S1** and the fit curves are shown in Fig. 3d. This shows that IBAI treatment not only reduces the level of PbI_2 and δ-$FAPbI_3$ near the surface but it also efficiently passivates electronic trap states likely caused by these impurities at or near the surface of the perovskite film. This improvement in the optoelectronic film quality has an impact on the device performance and in particular in the V_{oc} as will be shown in the following.

Photovoltaic performance and operational stability

In order to investigate the potential impact of combining the stepwise annealing with the introduction of a 2D-$IBA_2FAPb_2I_7$ layer on the photovoltaic performance we fabricated PSCs of the architecture FTO/compact-TiO_2/mesoscopic-TiO_2/perovskite/2D-layer/spiro-OMeTAD/gold (**Figure S10**). Representative *J-V* curves of PSCs with and without 2D $IBA_2FAPb_2I_7$ perovskite layer are shown in **Figure 4a,** from which we deduce the photovoltaic metrics summarized in **Table 2**. The device using neat $FAPbI_3$, subjected to treatment with MACl and stepwise sintering, showed a PCE of 20.4% with a V_{OC} of 1053 mV, a J_{SC} of 25.87 mA cm^{-2} and a fill factor of 0.772. Covering the perovskite film with the 2D-$IBA_2FAPb_2I_7$ layer enhances substantially all three PV metrics, the champion PSC achieving a PCE of 22.7%, with Voc = 1112 mV, J_{SC} =25.4 mA cm^{-2} and FF = 80.5%, which is one of the best efficiency values reported for all-iodide $FAPbI_3$-based PSCs. We attribute the increase in the V_{OC}, i.e. ΔV_{OC} = 191 mV and 59 mV with regards to bare $FAPbI_3$ films, with and without stepwise annealing, respectively, as well as the outstanding FF of 80.5% to the effective suppression of δ-$FAPbI_3$ phase formation together with the surface trap mitigation effect of the $IBA_2FAPb_2I_7$ overlayer. The surface treatment of the $FAPbI_3$ perovskite with IBAI converts most of the δ-$FAPbI_3$ into the 2D $IBA_2FAPb_2I_7$ surface layer, any residue being below the detection limit of our GIWAXS measurements. The removal of δ-$FAPbI_3$ prolongs the charge carrier lifetime as revealed by the TRPL measurements, enabling the high V_{OC} values observed for PSCs that are endowed with an α-$FAPbI_3$/$IBA_2FAPb_2I_7$ overlayer (*35*). In addition, the photovoltaic performance of *n*-butyl ammonium iodide (BAI) surface treated $FAPbI_3$ based perovskite is summarized in **Figure S11**. Champion cell with BAI treatment yielded PCE up to 21.8%, as compared to 22.7% with IBAI treatment and 20.4% untreated. The statistic results prove superior photovoltaic performance of IBAI treated PSC as compared to BAI.

The inset of **Figure 4a** shows the tracking of the maximum power point (MPPT) for two cells with and without 2D-overlayer over the first 60 seconds. The power output (SPO) of the device endowed with the 2D layer reached stabilized value of ~22.4%. within 10 s This yields an SPO-to-PCE ratio of 0.99, implying a reliable solar energy output (*36*). Statistics of photovoltaic parameters corresponding to $IBA_2FAPb_2I_7$ layer–based PSCs are summarized and compared with those obtained for 2D-layer free PSCs in **Figure 4c**. Enhanced V_{OC}, *FF*, and PCE values were obtained for over 25 perovskite devices endowed $IBA_2FAPb_2I_7$ overlayers, further revealing the effectiveness of using the 2D layer for passivating defects and for improving the photovoltaic performance.

Figure 4b shows incident photon to electron conversion efficiency (IPCE) spectra of PSCs with and without $IBA_2FAPb_2I_7$ surface treatment layer. The integrated photocurrents are in excellent agreement with *J-V* measurements, their difference being <2%. To evaluate the effects of the film treatment on the long-term device stability, we recoride the operational stability of the PSCs by exposing unsealed devices at room temperature to full-sun illumination in flowing nitrogen gas while tracking their MPP (**Figure 4d**). After 700 h, $FAPbI_3$ PSC endowed with the 2D $IBA_2FAPb_2I_7$

layer retained over 95% of its initial efficiency, proving excellent operational stability. In comparison, MACl treated PSCs without $IBA_2FAPb_2I_7$ surface layer retained merely 76% of their initial efficiency. To further substantiate the superior operational stability of $FAPbI_3$-based PSCs, we also performed MPP tracking experiment under simulated full-sun irradiance at 80 ºC for $FAPbI_3$–based PSC with and without 2D $IBA_2FAPb_2I_7$ layer. (**Figure 4e**). After over 500 h, the cell using a 2D $IBA_2FAPb_2I_7$ overlayer retained 84% of its initial efficiency while the PCE of the bare $FAPbI_3$ dropped to less than 26 % . The a robust performance of α-$FAPbI_3$/$IBA_2FAPb_2I_7$-based PSCs results from the suppression of the δ-$FAPbI_3$ phase, better perovskite film quality, and superior moisture stability of α-$FAPbI_3$/$IBA_2FAPb_2I_7$ layer (Figure **S12**) (*36-38*). $FAPbI_3$ films produced without the stepwise annealing and MACl treatment degrade severely within the first few hours of aging. Thus the new results obtained in our study set new benchmarks in terms of both efficiency and stability for $FAPbI_3$ –based PSCs.

Table 2. Photovoltaic parameters of PSCs based on stepwise annealing $FAPbI_3$ and $FAPbI_3$/IBAI (measured under simulated AM 1.5G solar irradiance at 100 mW cm^{-2}).

Device	V_{OC} (mV)	J_{SC} (mA cm^{-2})	*FF* (%)	*PCE* (%)
$FAPbI_3$	1053 (1043)*	25.87 (25.41)	77.2 (75.6)	20.4(20.1)
$FAPbI_3$/IBAI	1113 (1093)	25.83 (25.36)	80.5 (79.2)	22.7(22.1)

*The brackets indicate the average values of 10 PSC devices for $FAPbI_3$, and 25 PSC devices for α-$FAPbI_3$/$IBA_2FAPb_2I_7$.

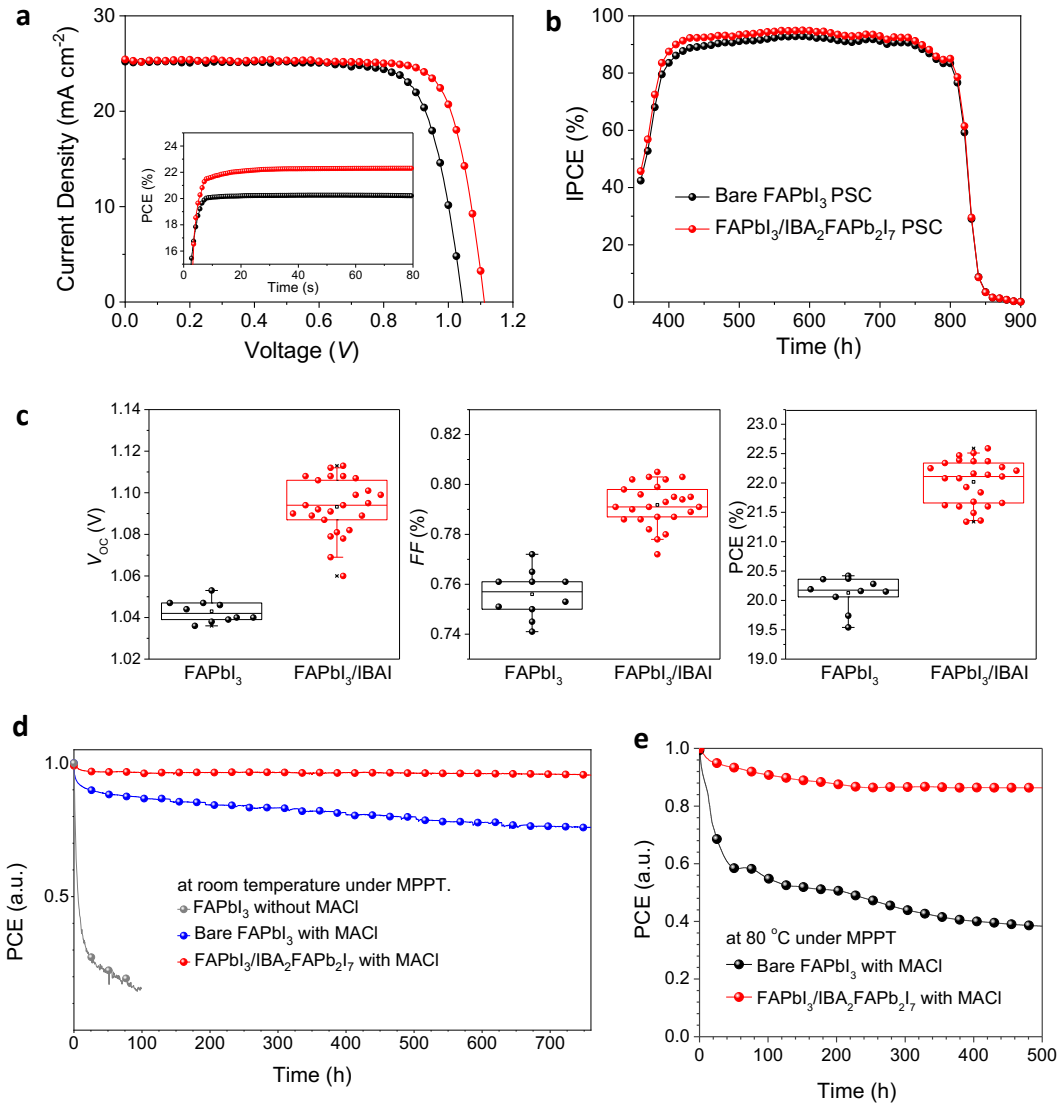

Figure 4. Photovoltaic and stability measurements: JV curves (**a**), IPCE curves (**b**), V_{OC}, FF and PCE matrix (**c**), ageing results (**d**) and (**e**) of PSCs based on bare $FAPbI_3$ (black dotted line) α-$FAPbI_3/IBA_2FAPb_2I_7$ perovskites (red dotted line). The inset of Figure 4a shows the MPP tracking data of PSCs based on bare $FAPbI_3$ and α-$FAPbI_3/IBA_2FAPb_2I_7$ perovskites.

Conclusions

In conclusion, using a stepwise annealing method, $FAPbI_3$ –based perovskites have been stabilized by effectively suppressing the formation of δ-$FAPbI_3$ non-perovskite phase. By exploiting the catalytic activity of MACl together with surface coating of a molecularly tailored $IBA_2FAPb_2I_7$ layer, a PCE approaching 23% was achieved, which is amongst the highest values reported for pure $FAPbI_3$–based PSCs. Such 2D coated PSCs exhibited superior operational stability under a heat stress of 80 °C. Our work provides an efficient and cost-effective way to stabilize and to improve the operational stability of $FAPbI_3$ –based perovskite, paving the way for the industrialization of PSCs.

Acknowledgement

Y.L. S.M.Z., and M.G. thank the King Abdulaziz City for Science and Technology (KACST) and the European Union's Horizon 2020 research and innovation program (grant agreement No 826013) for financial support. The authors thank Mr. Aditya Mishra, Dr. Michael Hope and Prof. Lyndon Emsley for their help on solid-state NMR research.

1. NREL, Best research efficiencies: Https://www.Nrel.Gov/pv/assets/images/efficiencychart.Png.
2. A. Kojima, K. Teshima, Y. Shirai, T. Miyasaka, Organometal halide perovskites as visible-light sensitizers for photovoltaic cells. *J. Am. Chem. Soc.* **131**, 6050-6051 (2009).
3. D. Bi, C. Yi, J. Luo, J.-D. Décoppet, F. Zhang, S. M. Zakeeruddin, X. Li, A. Hagfeldt, M. Grätzel, Polymer-templated nucleation and crystal growth of perovskite films for solar cells with efficiency greater than 21%. *Nat. Energy* **1**, 16142 (2016).
4. W. S. Yang, B.-W. Park, E. H. Jung, N. J. Jeon, Y. C. Kim, D. U. Lee, S. S. Shin, J. Seo, E. K. Kim, J. H. Noh, Iodide management in formamidinium-lead-halide–based perovskite layers for efficient solar cells. *Science* **356**, 1376-1379 (2017).
5. Y. Zhao, K. Zhu, Organic–inorganic hybrid lead halide perovskites for optoelectronic and electronic applications. *Chem. Soc. Rev.* **45**, 655-689 (2016).
6. S. Akin, Y. Altintas, E. Mutlugun, S. Sonmezoglu, Cesium-lead based inorganic perovskite quantum-dots as interfacial layer for highly stable perovskite solar cells with exceeding 21% efficiency. *Nano Energy* **60**, 557-566 (2019).
7. J.-Y. Seo, H.-S. Kim, S. Akin, M. Stojanovic, E. Simon, M. Fleischer, A. Hagfeldt, S. M. Zakeeruddin, M. Grätzel, Novel p-dopant toward highly efficient and stable perovskite solar cells. *Energ Environ Sci* **11**, 2985-2992 (2018).
8. T. Leijtens, G. E. Eperon, N. K. Noel, S. N. Habisreutinger, A. Petrozza, H. J. Snaith, Stability of metal halide perovskite solar cells. *Adv. Energy Mater.* **5**, 1500963 (2015).
9. A. J. Pearson, G. E. Eperon, P. E. Hopkinson, S. N. Habisreutinger, J. T. W. Wang, H. J. Snaith, N. C. Greenham, Oxygen degradation in mesoporous al2o3/ch3nh3pbi3-xclx perovskite solar cells: Kinetics and mechanisms. *Adv. Energy Mater.* **6**, 1600014 (2016).
10. N. Arora, M. I. Dar, A. Hinderhofer, N. Pellet, F. Schreiber, S. M. Zakeeruddin, M. Grätzel, Perovskite solar cells with cuscn hole extraction layers yield stabilized efficiencies greater than 20%. *Science*, eaam5655 (2017).
11. A. Mei, X. Li, L. Liu, Z. Ku, T. Liu, Y. Rong, M. Xu, M. Hu, J. Chen, Y. Yang, M. Gtätzel, H. Han, A hole-conductor–free, fully printable mesoscopic perovskite solar cell with high stability. *Science* **345**, 295-298 (2014).
12. B. Conings, J. Drijkoningen, N. Gauquelin, A. Babayigit, J. D'Haen, L. D'Olieslaeger, A. Ethirajan, J. Verbeeck, J. Manca, E. Mosconi, Intrinsic thermal instability of methylammonium lead trihalide perovskite. *Advanced Energy Materials* **5**, 1500477 (2015).
13. S.-H. Turren-Cruz, A. Hagfeldt, M. Saliba, Methylammonium-free, high-performance, and stable perovskite solar cells on a planar architecture. *Science* **362**, 449-453 (2018).
14. Y. Rong, Y. Hu, A. Mei, H. Tan, M. I. Saidaminov, S. I. Seok, M. D. McGehee, E. H. Sargent, H. Han, Challenges for commercializing perovskite solar cells. *Science* **361**, eaat8235 (2018).
15. J. Burschka, N. Pellet, S. J. Moon, R. Humphry-Baker, P. Gao, M. K. Nazeeruddin, M. Gratzel, Sequential deposition as a route to high-performance perovskite-sensitized solar cells.

Nature **499**, 316-319 (2013).

16. N. J. Jeon, J. H. Noh, W. S. Yang, Y. C. Kim, S. Ryu, J. Seo, S. I. Seok, Compositional engineering of perovskite materials for high-performance solar cells. *Nature* **517**, 476 (2015).
17. M. M. Lee, J. Teuscher, T. Miyasaka, T. N. Murakami, H. J. Snaith, Efficient hybrid solar cells based on meso-superstructured organometal halide perovskites. *Science*, 1228604 (2012).
18. H. S. Kim, C. R. Lee, J. H. Im, K. B. Lee, T. Moehl, A. Marchioro, S. J. Moon, R. Humphry-Baker, J. H. Yum, J. E. Moser, M. Gratzel, N. G. Park, Lead iodide perovskite sensitized all-solid-state submicron thin film mesoscopic solar cell with efficiency exceeding 9%. *Sci. Rep.* **2**, 591 (2012).
19. Y. Liu, S. Akin, L. Pan, R. Uchida, N. Arora, J. V. Milić, A. Hinderhofer, F. Schreiber, A. R. Uhl, S. M. Zakeeruddin, A. Hagfeldt, M. I. Dar, M. Grätzel, Ultrahydrophobic 3d/2d fluoroarene bilayer-based water-resistant perovskite solar cells with efficiencies exceeding 22%. *Sci Adv* **5**, eaaw2543 (2019).
20. H.-S. Kim, J.-Y. Seo, S. Akin, E. Simon, M. Fleischer, S. M. Zakeeruddin, M. Graetzel, A. Hagfeldt, Power output stabilizing feature in perovskite solar cells at operating condition: Selective contact-dependent charge recombination dynamics. *Nano Energy* **61**, 126-131 (2019).
21. N. Pellet, P. Gao, G. Gregori, T.-Y. Yang, M. K. Nazeeruddin, J. Maier, M. Grätzel, Mixed-organic-cation perovskite photovoltaics for enhanced solar-light harvesting. *Angew. Chem. Int. Ed.* **53**, 3151-3157 (2014).
22. W. Liao, D. Zhao, Y. Yu, N. Shrestha, K. Ghimire, C. R. Grice, C. Wang, Y. Xiao, A. J. Cimaroli, R. J. Ellingson, Fabrication of efficient low-bandgap perovskite solar cells by combining formamidinium tin iodide with methylammonium lead iodide. *Journal of the American Chemical Society* **138**, 12360-12363 (2016).
23. D. Zhao, Y. Yu, C. Wang, W. Liao, N. Shrestha, C. R. Grice, A. J. Cimaroli, L. Guan, R. J. Ellingson, K. Zhu, Low-bandgap mixed tin–lead iodide perovskite absorbers with long carrier lifetimes for all-perovskite tandem solar cells. *Nature Energy* **2**, 17018 (2017).
24. C. Yi, J. Luo, S. Meloni, A. Boziki, N. Ashari-Astani, C. Grätzel, S. M. Zakeeruddin, U. Röthlisberger, M. Grätzel, Entropic stabilization of mixed a-cation abx 3 metal halide perovskites for high performance perovskite solar cells. *Energy & Environmental Science* **9**, 656-662 (2016).
25. Z. Wang, Y. Zhou, S. Pang, Z. Xiao, J. Zhang, W. Chai, H. Xu, Z. Liu, N. P. Padture, G. Cui, Additive-modulated evolution of hc (nh2) 2pbi3 black polymorph for mesoscopic perovskite solar cells. *Chemistry of Materials* **27**, 7149-7155 (2015).
26. T. Niu, J. Lu, M.-C. Tang, D. Barrit, D.-M. Smilgies, Z. Yang, J. Li, Y. Fan, T. Luo, I. McCulloch, High performance ambient-air-stable fapbi 3 perovskite solar cells with molecule-passivated ruddlesden–popper/3d heterostructured film. *Energy & Environmental Science* **11**, 3358-3366 (2018).
27. W. S. Yang, J. H. Noh, N. J. Jeon, Y. C. Kim, S. Ryu, J. Seo, S. I. Seok, High-performance photovoltaic perovskite layers fabricated through intramolecular exchange. *Science* **348**, 1234-1237 (2015).
28. M. Kim, G.-H. Kim, T. K. Lee, I. W. Choi, H. W. Choi, Y. Jo, Y. J. Yoon, J. W. Kim, J. Lee, D. Huh, Methylammonium chloride induces intermediate phase stabilization for efficient

perovskite solar cells. *Joule*, (2019).

29. D. G. Billing, A. Lemmerer, Synthesis, characterization and phase transitions in the inorganic–organic layered perovskite-type hybrids [(cnh2n+ 1nh3) 2pbi4], n= 4, 5 and 6. *Acta Crystallogr. Sect. B: Struct. Sci.* **63**, 735-747 (2007).
30. M. T. Weller, O. J. Weber, J. M. Frost, A. Walsh, Cubic perovskite structure of black formamidinium lead iodide, α-[hc (nh2) 2] pbi3, at 298 k. *The journal of physical chemistry letters* **6**, 3209-3212 (2015).
31. P. Gratia, I. Zimmermann, P. Schouwink, J.-H. Yum, J.-N. Audinot, K. Sivula, T. Wirtz, M. K. Nazeeruddin, The many faces of mixed ion perovskites: Unraveling and understanding the crystallization process. *ACS Energy Letters* **2**, 2686-2693 (2017).
32. C. C. Stoumpos, D. H. Cao, D. J. Clark, J. Young, J. M. Rondinelli, J. I. Jang, J. T. Hupp, M. G. Kanatzidis, Ruddlesden–popper hybrid lead iodide perovskite 2d homologous semiconductors. *Chemistry of Materials* **28**, 2852-2867 (2016).
33. Y. Cho, A. M. Soufiani, J. S. Yun, J. Kim, D. S. Lee, J. Seidel, X. Deng, M. A. Green, S. Huang, A. W. Y. Ho-Baillie, Mixed 3d–2d passivation treatment for mixed-cation lead mixed-halide perovskite solar cells for higher efficiency and better stability. *Advanced Energy Materials* **8**, 1703392 (2018).
34. H. Zhu, Y. Liu, F. T. Eickemeyer, L. Pan, D. Ren, M. A. Ruiz-Preciado, B. Carlsen, B. Yang, X. Dong, Z. Wang, H. Liu, S. Wang, S. M. Zakeeruddin, A. Hagfeldt, M. I. Dar, X. Li, M. Grätzel, Tailored amphiphilic molecular mitigators for stable perovskite solar cells with 23.5% efficiency. *Advanced Materials* **32**, 1907757 (2020).
35. W. Q. Wu, Z. B. Yang, P. N. Rudd, Y. C. Shao, X. Z. Dai, H. T. Wei, J. J. Zhao, Y. J. Fang, Q. Wang, Y. Liu, Y. H. Deng, X. Xiao, Y. X. Feng, J. S. Huang, Bilateral alkylamine for suppressing charge recombination and improving stability in blade-coated perovskite solar cells. *Sci Adv* **5**, eaav8925 (2019).
36. Z. P. Wang, Q. Q. Lin, F. P. Chmiel, N. Sakai, L. M. Herz, H. J. Snaith, Efficient ambient-air-stable solar cells with 2d-3d heterostructured butylammonium-caesium-formamidinium lead halide perovskites. *Nat Energy* **2**, 17135 (2017).
37. G. Grancini, C. Roldan-Carmona, I. Zimmermann, E. Mosconi, X. Lee, D. Martineau, S. Narbey, F. Oswald, F. De Angelis, M. Graetzel, M. K. Nazeeruddin, One-year stable perovskite solar cells by 2d/3d interface engineering. *Nat Commun* **8**, 15684 (2017).
38. J. W. Lee, Z. H. Dai, T. H. Han, C. Choi, S. Y. Chang, S. J. Lee, N. De Marco, H. X. Zhao, P. Y. Sun, Y. Huang, Y. Yang, 2d perovskite stabilized phase-pure formamidinium perovskite solar cells. *Nat Commun* **9**, 3021 (2018).